Available online at www.sciencedirect.com
ScienceDirect
Journal of Power Sources 166 (2007) 127–136
JOURNAL OF POWER SOURCES
www.elsevier.com/locate/jpowsour

Hydrogen production through steam electrolysis: Model-based steady state performance of a cathode-supported intermediate temperature solid oxide electrolysis cell

J. Udagawa [a,b], P. Aguiar [b], N.P. Brandon [b,*]

[a] *Imperial Centre for Energy Policy and Technology, Centre for Environmental Policy, Imperial College London, London SW7 2AZ, UK*
[b] *Department of Earth Science and Engineering, Imperial College London, London SW7 2AZ, UK*

Received 4 October 2006; received in revised form 11 December 2006; accepted 27 December 2006
Available online 16 January 2007

Abstract

Hydrogen production via steam electrolysis may involve less electrical energy consumption than conventional low temperature water electrolysis, reflecting the improved thermodynamics and kinetics at elevated temperatures. The present paper reports on the development of a one-dimensional dynamic model of a cathode-supported planar intermediate temperature solid oxide electrolysis cell (SOEC) stack. The model, which consists of an electrochemical model, a mass balance, and four energy balances, is here employed to study the steady state behaviour of an SOEC stack at different current densities and temperatures. The simulations found that activation overpotentials provide the largest contributions to irreversible losses while concentration overpotentials remained negligible throughout the stack. For an average current density of 7000 A m^{-2} and an inlet steam temperature of 1023 K, the predicted electrical energy consumption of the stack is around 3 kW h per normal m^3 of hydrogen, significantly smaller than those of low temperature stacks commercially available today. However, the dependence of the stack temperature distribution on the average current density calls for strict temperature control, especially during dynamic operation.

Keywords: Hydrogen production; Steam electrolyser; SOEC; Intermediate temperature; Planar; Dynamic model

1. Introduction

Hydrogen is regarded as a leading candidate for alternative future fuels. It has the potential to address the environmental and energy security issues associated with fossil-derived hydrocarbon fuels. Among many hydrogen production methods, water electrolysis is a well-established technique, which is capable of producing emissions-free hydrogen if used in conjunction with renewable or nuclear energy. However, water electrolysis has not had a significant commercial penetration, mainly due to its high electricity consumption and thus high operating or running cost [1].

Steam electrolysis at elevated temperatures might offer a solution by consuming less electricity than is required at ambient conditions. The minimum energy consumption during steam electrolysis is evaluated as a function of temperature in Fig. 1, using thermodynamic tables [2]. Here the gas compositions are taken to be 50 mol% H_2 / 50 mol% H_2O and 100 mol% O_2. In the figure, $T\Delta S$ and ΔG represent, respectively, the thermal and electrical energies consumed in the reaction, while ΔH corresponds to the total energy consumption, in the absence of irreversible losses. Although ΔH remains approximately constant, ΔG tends to decrease and $T\Delta S$ tends to increase as the temperature is raised, providing more opportunities to apply waste heat from other processes, or to make effective use of the heat generated via irreversible losses. At 1273 K, almost 30% of the total energy consumption can be satisfied through the supply of thermal energy alone. The increase in temperature can also eliminate the need for expensive catalysts, which may be required for some low temperature water electrolysers [3]. However, in the design of a solid oxide electrolysis cell (SOEC), there are other factors that need to be taken into account, which influence the performance of the actual device as will be explained in the following sections.

Steam electrolysis is performed using an SOEC, which can be seen in simple terms as the reverse operation of a solid oxide fuel

* Corresponding author. Tel.: +44 20 7594 5704; fax: +44 20 7594 7444.
E-mail address: n.brandon@imperial.ac.uk (N.P. Brandon).

0378-7753/$ – see front matter © 2007 Elsevier B.V. All rights reserved.
doi:10.1016/j.jpowsour.2006.12.081

Nomenclature

C_{H_2}, C_{H_2O} concentration of hydrogen and steam in the cathode gas stream (mol m^{-3})
C_i concentration of gas species i in the cathode and anode gas streams (mol m^{-3})
$C_{p,C}$, $C_{p,A}$, $C_{p,S}$, $C_{p,I}$ heat capacity of the cathode and anode gas streams, solid structure and interconnect (J kg^{-1} K^{-1})
C_i^0 concentration of gas species i at the cell inlet (mol m^{-3})
$C_{H_2}^{TPB}$, $C_{H_2O}^{TPB}$ concentration of hydrogen and steam at the triple phase boundary (mol m^{-3})
$d_{h,C}$, $d_{h,A}$ hydraulic diameter of the cathode and anode gas channels (m)
$D_{eff,cathode}$ average effective diffusivity coefficient of the cathode (m^2 s^{-1})
$E_{cathode}$, E_{anode} activation energy for the exchange current density of the cathode and anode (J mol^{-1})
$E_{electrode}$ activation energy for the exchange current density of an electrode (J mol^{-1})
F Faraday's constant (C mol^{-1})
ΔG Gibbs free energy change of the reaction (J mol^{-1} H_2)
h_C, h_A, h_S, h_I height of the cathode and anode channels, and thickness of the solid structure and interconnect (m)
ΔH enthalpy change of the reaction (J mol^{-1} H_2)
j local current density (A m^{-2})
$j_{0,cathode}$, $j_{0,anode}$ exchange current density of the cathode and anode (A m^{-2})
$j_{0,electrode}$ exchange current density of an electrode (A m^{-2})
k_C, k_A convective heat transfer coefficient between the solid parts of the cell and the cathode and anode gas streams (J m^{-2} s^{-1} K^{-1})
$k_{cathode}$, k_{anode} pre-exponential factor for the exchange current density of the cathode and anode (Ω^{-1} m^{-2})
$k_{electrode}$ pre-exponential factor for the exchange current density of an electrode (Ω^{-1} m^{-2})
L cell length (m)
Nu_C, Nu_A Nusselt number of the cathode and anode gas streams
P_{O_2} oxygen pressure in the anode gas stream (Pa)
$P_{O_2}^{TPB}$ oxygen pressure at the triple phase boundary (Pa)
R reaction rate (mol s^{-1} m^{-2})
R_{Ohm} total resistance of the cell including electric and ionic resistances (Ω m^2)
$\Re$ gas constant (J mol^{-1} K^{-1})
ΔS entropy change of the reaction (J K^{-1} mol^{-1} H_2)
t time (s)
T temperature (K)
T_C, T_A, T_S, T_I temperature of the cathode and anode gas streams, solid structure and interconnect (K)
T_C^0 temperature of the cathode gas stream at the inlet (K)
u_C, u_A velocity of the cathode and anode gas streams (m s^{-1})
U cell potential (V)
U^0 standard potential (V)
U^{rev} reversible potential (V)
$U^{rev,TPB}$ reversible potential estimated for the gas concentrations at the triple phase boundary (V)
W cell width (m)
x axial coordinate (m)

Greek letters
α transfer coefficient
ε_S, ε_I emissivity of the solid structure and interconnect
$\eta_{act,cathode}$, $\eta_{act,anode}$ activation overpotential losses at the cathode and anode (V)
η_{conc} total concentration overpotential losses (V)
$\eta_{conc,cathode}$, $\eta_{conc,anode}$ concentration overpotential losses at the cathode and anode (V)
η_{Ohm} Ohmic losses (V)
η_{total} total irreversible losses (V)
λ_C, λ_A, λ_S, λ_I thermal conductivity of the cathode and anode gas streams, solid structure and interconnect (J m^{-1} s^{-1} K^{-1})
ν_i stoichiometric coefficient of gas species i
ρ_C, ρ_A, ρ_S, ρ_I density of the cathode and anode gas streams, solid structure and interconnect (kg m^{-3})
σ Stefan–Boltzmann constant (W m^{-2} K^{-4})
$\sigma_{cathode}$, σ_{anode} electric conductivity of the cathode and anode (Ω^{-1} m^{-1})
$\sigma_{electrolyte}$ ionic conductivity of the electrolyte (Ω^{-1} m^{-1})
$\tau_{cathode}$, $\tau_{electrolyte}$, τ_{anode} thickness of the cathode, electrolyte and anode (m)

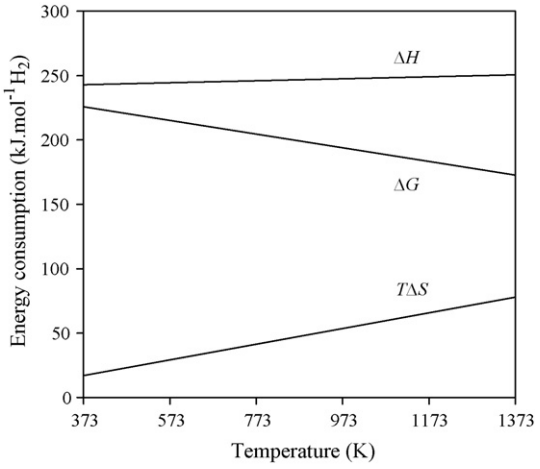

Fig. 1. Thermal ($T\Delta S$), electrical (ΔG) and total (ΔH) energy consumption during steam electrolysis as a function of temperature. The gas compositions are taken to be 50 mol% H_2/50 mol% H_2O and 100 mol% O_2. Irreversible losses are not taken into account.

Table 1
Chemical reactions involved in an SOEC

Cathode	$H_2O + 2e^- \rightarrow H_2 + O^{2-}$
Anode	$O^{2-} \rightarrow \frac{1}{2}O_2 + 2e^-$
Overall	$H_2O \rightarrow H_2 + \frac{1}{2}O_2$

cell, allowing for the opportunity to apply recent developments in SOFCs to the field. An SOEC consists of a three-layer solid structure (composed of porous cathode, electrolyte and porous anode) and an interconnect plate. Steam is introduced at the cathode side of the solid structure where it is reduced into hydrogen, releasing oxide ions in the process. The oxide ions then migrate through the electrolyte to the anode where they combine to form oxygen molecules, releasing electrons. The balanced chemical equations for the reactions are shown in Table 1. Although the use of proton conductors has also been investigated [4–6], yttria-stabilised zirconia (YSZ), which is an oxide ion conductor, is generally used for the electrolyte in SOECs. Typical materials for the cathode are nickel–YSZ cermets and those for the anode are perovskite oxides such as lanthanum manganite.

In SOFC technologies, there is increased interest in intermediate temperature SOFCs (IT-SOFCs), which typically operate between 823 and 1073 K, to allow for a wider range of materials, more cost effective SOFC fabrication [7] and increased durability. The reduction in operating temperature has also been seen in the field of SOECs in the limited number of experimental projects reported over the recent decades [8–10], where the temperature at which the cells are tested has decreased from 1273 to 1073 K. Initially SOECs were developed as tubular cell structures to avoid sealing problems, which is a major issue in segregating the produced H_2 and O_2 in planar cells, particularly over multiple thermal cycles [11]. Today, despite such sealing difficulties, the trend in cell design is to employ planar structures. A planar structure permits high packing density and significantly smaller hot volume in the system than that allowed by a tubular design [10]. The main motivation behind the use of planar cells is, however, the low manufacturing cost [12]. The planar design also allows for shorter current path, reducing the Ohmic resistance within the cell [12]. A planar SOEC can be categorised as being either an electrolyte-supported or electrode-supported design. The former employs the electrolyte as the support structure and is suitable for high temperature operation in which the, often large, Ohmic resistance associated with a thick electrolyte can be reduced. In an electrode-supported cell, on the other hand, one of the electrodes is the thickest part of the solid structure. Such a design has been developed in order to minimise Ohmic resistances in SOFCs operating at intermediate temperatures and may also be applied to intermediate temperature SOECs (IT-SOECs).

A mathematical model is an important design tool for such devices as an SOEC, which are still in the development stage. It allows the prediction of the behaviour of the device under different process conditions and assists in the optimisation of its performance. In particular, such a model is essential in understanding the response of an electrolyser under steady electrical power input, such as those from the grid or nuclear energy, as well as under an intermittent renewable electrical power input. The present paper reports the development of a dynamic model of a conceptual IT-SOEC produced within the gPROMS modelling environment [13]. The paper introduces the IT-SOEC model and the results describing the simulated steady state behaviour of such an electrolyser. Issues related to thermal management of the cell are discussed. In spite of the model's dynamic capability, only the steady state results are discussed here. The dynamic response will be presented in a subsequent publication.

2. IT-SOEC mathematical model

Today, although studies on the thermodynamics of electrolysis at elevated temperatures can be found in several publications [9,14,15], mathematical modelling of an SOEC stack is still not an active area of research. To the authors' knowledge, neither results related to the spatially distributed stack performance nor the transient behaviour of a stack have been published. Here, a previously developed dynamic model of an anode-supported planar IT-SOFC stack [7,16] has been modified to produce a one-dimensional model for a planar IT-SOEC stack that operates across a wide range of temperatures, using a thick film YSZ electrolyte in a cathode-supported cell configuration.

To ensure a sufficient rate of H_2 production, an SOEC system must consist of several repeating cells assembled in stacks. However, the models of such stacks are usually constructed for the smallest unit cell, which is assumed to describe the response of the whole stack subject to the use of adequate boundary conditions. Here, the modelled unit cell is considered to be in the centre of a large stack such that there are no end effects. Although interconnects normally provide the gas flow channels, above and below the solid structure, the effect of individual passages is here neglected. The pressure drop along the gas channels is also assumed negligible at the operating pressure of 0.1 MPa. For the purpose of modelling, the unit cell is considered to be composed of four components, the cathode and anode gas streams, solid structure and interconnect. Fig. 2 shows the schematic view of such a unit cell. The model developed consists of an electrochemical model, a mass balance for the cathode stream, and four energy balances for the cathode and anode streams, solid

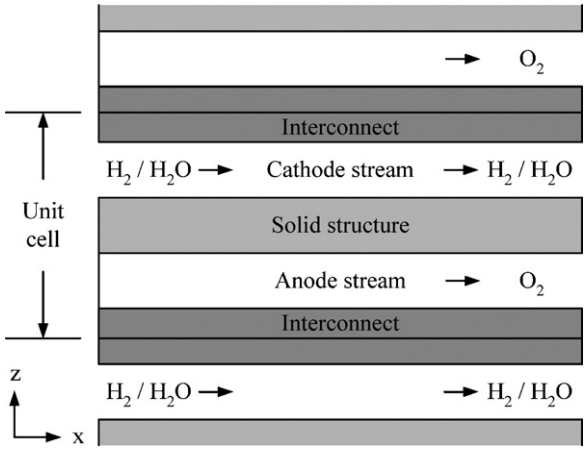

Fig. 2. Schematic view of a planar SOEC stack.

structure and interconnect. In spite of the temperature gradient expected along the cell, the properties of the gas streams, solid structure and interconnect are assumed to be constant in order to achieve a more computationally tractable model. This assumption is reported valid for the previously developed IT-SOFC model during steady state simulations [17] and is thus also considered applicable for the IT-SOEC model. Finally, ideal gas behaviour is assumed for the cathode and anode streams where appropriate.

2.1. Electrochemical model

An electrochemical model is used to relate such variables as gas species concentrations, cell component temperatures and average current density to the electrical potential of the cell, which can then be used to calculate the electrical energy consumption. The electrical potential is taken as constant along the cell as the electrodes are assumed to be good electric conductors, and thus it is not a local quantity. As shown in Eq. (1), the cell potential corresponds to the sum of the reversible potential and all the irreversible losses that occur as the electrical current is passed through the cell. Such irreversible losses include Ohmic losses, concentration overpotentials and activation overpotentials, which are all partly responsible for the heat produced within the cell. In general, irreversible losses are dominated at high current densities by concentration overpotentials and at low current densities by activation overpotentials.

$$U = U^{\text{rev}}(x) + \eta_{\text{Ohm}}(x) + \eta_{\text{conc,cathode}}(x) + \eta_{\text{conc,anode}}(x) + \eta_{\text{act,cathode}}(x) + \eta_{\text{act,anode}}(x) \quad (1)$$

The reversible potential is determined through the Nernst equation, which predicts the minimum electrical potential required to split H_2O at a particular location along the cell with a specific temperature and gas concentrations. Eq. (2) has been derived assuming ideal gas behaviour. The solid structure temperature is applied in the Nernst equation as the reactions take place at the triple phase boundaries (TPBs) where the electrolyte, porous electrode and gas species meet at the interfaces between the electrolyte and the electrodes. U^0 represents the standard potential, which corresponds to the reversible potential calculated at unity activity. It is determined as a function of the Gibbs free energy change involved in the reaction, taking the partial pressures of H_2, H_2O and O_2 to be at standard pressure.

$$U^{\text{rev}}(x) = U^0(x) + \frac{\Re T_S(x)}{2F} \ln\left[\frac{C_{H_2}(x)[P_{O_2} \times 10^{-5}]^{0.5}}{C_{H_2O}(x)}\right] \quad (2)$$

2.1.1. Ohmic losses

Ohmic losses originate from the resistance to the conduction of ions through the electrolyte and electrons through the electrodes and interconnect, as well as from the contact resistances, which exist between cell components. Ohmic losses are linearly proportional to the current density and can be determined through Ohm's law as shown in Eq. (3), where j and R_{Ohm} represent the local current density and local cell resistance, respectively. R_{Ohm} is calculated using the conductivity data of each layer of the solid structure. In Eq. (4), cross plane charge flow and series connection of resistances have been assumed [7]. The resistance through the interconnect and the contact resistances are considered negligible. The conductivity of the electrodes are assumed constant along the cell while that of the electrolyte is estimated as a function of local temperature [18].

$$\eta_{\text{Ohm}}(x) = j(x)R_{\text{Ohm}}(x) \quad (3)$$

$$R_{\text{Ohm}}(x) = \frac{\tau_{\text{cathode}}}{\sigma_{\text{cathode}}} + \frac{\tau_{\text{electrolyte}}}{\sigma_{\text{electrolyte}}(x)} + \frac{\tau_{\text{anode}}}{\sigma_{\text{anode}}} \quad (4)$$

2.1.2. Concentration overpotential losses

Concentration overpotentials occur if mass transport of the gas species involved in the reaction becomes the limiting factor. When current is flowing in the cell, reactant H_2O is consumed and product H_2 and O_2 are formed at the TPBs. If the fluxes of the reactant to, and the products away from, the TPBs are slower than that corresponding to the discharged electrical current, concentration gradients for the species develop in the porous electrode. The concentration overpotentials are the result of such concentration gradients causing the actual reversible potential at the TPBs, shown in Eq. (5), to deviate from the reversible potential predicted by the Nernst Eq. (2) using bulk concentrations in the cathode and anode streams. High current densities and high steam utilisation factors can contribute in creating significant concentration overpotentials.

$$U^{\text{rev,TPB}}(x) = U^0(x) + \frac{\Re T_S(x)}{2F} \ln\left[\frac{C^{\text{TPB}}_{H_2}(x)[P^{\text{TPB}}_{O_2} \times 10^{-5}]^{0.5}}{C^{\text{TPB}}_{H_2O}(x)}\right] \quad (5)$$

$$\eta_{\text{conc}}(x) = \frac{\Re T_S(x)}{2F} \ln\left[\frac{C^{\text{TPB}}_{H_2}(x)C_{H_2O}(x)}{C_{H_2}(x)C^{\text{TPB}}_{H_2O}(x)}\right] + \frac{\Re T_S(x)}{4F} \ln\left[\frac{P^{\text{TPB}}_{O_2}}{P_{O_2}}\right] \quad (6)$$

The difference between Eqs. (2) and (5) corresponds to the concentration overpotential (6) where the first and second terms on the right hand side represent the concentration overpotential at the cathode and anode, respectively. The cathode concentration overpotential is presented separately in Eq. (7) while the anode concentration overpotential is not considered here, assuming the difference between the O_2 pressure at the TPBs and that in the bulk stream to be negligible. Eqs. (8) and (9) show the TPB concentrations, determined for equimolar counter-current one-dimensional diffusion of H_2 and H_2O. $D_{\text{eff,cathode}}$ represents the average effective diffusivity coefficient in the cathode, considering a binary gas mixture of H_2 and H_2O. A method for expressing the mass diffusion activities in an SOFC [19,20] has been adopted for an SOEC in deriving Eqs. (8) and (9).

$$\eta_{\text{conc,cathode}}(x) = \frac{\Re T_S(x)}{2F} \ln\left[\frac{C^{\text{TPB}}_{H_2}(x)C_{H_2O}(x)}{C_{H_2}(x)C^{\text{TPB}}_{H_2O}(x)}\right] \quad (7)$$

Table 2
Pre-exponential factor and activation energy for the exchange current density

k_{cathode}	$654 \times 10^9\ \Omega^{-1}\ \text{m}^{-2}$	E_{cathode}	$140 \times 10^3\ \text{J mol}^{-1}$
k_{anode}	$235 \times 10^9\ \Omega^{-1}\ \text{m}^{-2}$	E_{anode}	$137 \times 10^3\ \text{J mol}^{-1}$

$$C_{H_2}^{TPB}(x) = C_{H_2}(x) + \frac{\tau_{\text{cathode}}}{2FD_{\text{eff,cathode}}} j(x) \tag{8}$$

$$C_{H_2O}^{TPB}(x) = C_{H_2O}(x) - \frac{\tau_{\text{cathode}}}{2FD_{\text{eff,cathode}}} j(x) \tag{9}$$

2.1.3. Activation overpotential losses

Activation overpotentials are related to the chemical kinetics of the reactions. They are classically determined through the Butler–Volmer equation. For the cathode activation overpotential, the extended form of the Butler–Volmer equation is applied in Eq. (10) to account for the differences in the gas concentrations at the TPBs and in the bulk stream. For the anode activation overpotential (11), the simplified form is used, as the difference between the O_2 concentration at TPBs and that in the bulk stream has been assumed negligible. Although reactions are generally rapid and activation overpotentials tend to be small at high temperatures, they can become the most significant form of irreversible losses as the operating temperature is reduced.

$$j(x) = j_{0,\text{cathode}}(x) \left[\frac{C_{H_2}^{TPB}(x)}{C_{H_2}(x)} \exp\left[\frac{2(1-\alpha)F}{\Re T_S(x)} \eta_{\text{act,cathode}}(x) \right] - \frac{C_{H_2O}^{TPB}(x)}{C_{H_2O}(x)} \exp\left[\frac{-2\alpha F}{\Re T_S(x)} \eta_{\text{act,cathode}}(x) \right] \right] \tag{10}$$

$$j(x) = j_{0,\text{anode}}(x) \left[\exp\left[\frac{2(1-\alpha)F}{\Re T_S(x)} \eta_{\text{act,anode}}(x) \right] - \exp\left[\frac{-2\alpha F}{\Re T_S(x)} \eta_{\text{act,anode}}(x) \right] \right] \tag{11}$$

α (usually taken to be 0.5), $j_{0,\text{cathode}}$ and $j_{0,\text{anode}}$ represent the transfer coefficient and the exchange current density for the cathode and anode, respectively. Electrode exchange current densities are expressed in Eq. (12) as a function of the pre-exponential factor and activation energy. Here it was assumed that in an SOEC, the forward and backward reactions at each electrode as well as the electrode materials are the reverse of those in an SOFC. Hence the values used for k_{anode} and E_{anode} in previous IT-SOFC studies have been substituted into k_{cathode} and E_{cathode} in the IT-SOEC model. The same assumption is used when assigning the values to the IT-SOEC anode kinetic parameters. The parameters employed for the IT-SOEC simulations are shown in Table 2.

$$j_{0,\text{electrode}}(x) = \frac{\Re T_S(x)}{2F} k_{\text{electrode}} \exp\left[\frac{-E_{\text{electrode}}}{\Re T_S(x)} \right] \tag{12}$$

$\text{electrode} \in \{\text{cathode, anode}\}$

2.2. Mass balance

The composition of the cathode stream evolves along the cell as the H_2/H_2O mixture moves towards the outlet. Such a composition change is tracked in the model using the cathode stream mass balance (13) and the boundary conditions at the cell inlet (14), predicting the H_2 and H_2O concentrations at each location along the channel. R represents the rate of reaction, which is related to the local current density through Faraday's law (15), assuming a current efficiency of 100%. As for the anode channel, it is assumed that any O_2 produced flows naturally out of the channel and thus there is no forced gas movement as in the cathode side. Therefore, the developed model does not consider an anode mass balance. Instead, the anode stream is modelled as a flow of pure O_2 at constant pressure along the cell. The cathode and anode stream velocities are assumed constant and determined from the outlet flow rate of the streams.

$$\frac{\partial}{\partial t}[C_i(x)] = -u_C \frac{\partial}{\partial x}[C_i(x)] + \frac{1}{h_C} \nu_i R(x), \quad i \in \{H_2, H_2O\} \tag{13}$$

$$C_i(0) = C_i^0, \quad i \in \{H_2, H_2O\} \tag{14}$$

$$R(x) = \frac{j(x)}{2F} \tag{15}$$

2.3. Energy balances

Eqs. (16)–(23) are used in predicting the temperatures of the cathode and anode streams, solid structure and interconnect. In Eqs. (16) and (18), the first term on the right hand side relates to the energy carried in the gas streams as they flow along the channels. The energy balances consider the thermal fluxes between the gas streams and the solid parts of the cell to be fully described by convection. The convective heat transfer coefficients for the cathode and anode streams (k_C and k_A) are calculated using Eq. (24), assuming constant Nusselt number and hydraulic diameter (25). In the cathode stream, k_C is assumed equivalent for both the convective heat transfer over the solid structure and interconnect surfaces. The same assumption is applied to k_A in the anode stream. The thermal fluxes along the solid parts of the cell are modelled using Fourier's law of heat conduction while radiative heat exchange is taken into account between the solid structure and interconnect. The entire enthalpy change of the reaction is assumed to occur in the solid structure. Mean density and mean heat capacity values are applied in the anode and cathode energy balances. These are calculated as spatial averages of all the values along the cell. The remaining gas and material properties are taken to be constant along the cell.

$$\frac{\partial}{\partial t}[T_C(x)] = -u_C \frac{\partial}{\partial x}[T_C(x)] + \frac{k_C}{\rho_C c_{p,C} h_C}[T_S(x) - T_C(x)] + \frac{k_C}{\rho_C c_{p,C} h_C}[T_I(x) - T_C(x)] \tag{16}$$

$$T_C(0) = T_C^0 \tag{17}$$

$$\frac{\partial}{\partial t}[T_A(x)] = -u_A\frac{\partial}{\partial x}[T_A(x)] + \frac{k_A}{\rho_A c_{p,A} h_A}[T_S(x) - T_A(x)] + \frac{k_A}{\rho_A c_{p,A} h_A}[T_I(x) - T_A(x)] \quad (18)$$

$$T_A(0) = \frac{T_s(0) + T_I(0)}{2} \quad (19)$$

$$\frac{\partial}{\partial t}[T_S(x)] = \frac{\lambda_S}{\rho_S c_{p,S}}\frac{\partial^2}{\partial x^2}[T_S(x)] - \frac{k_C}{\rho_S c_{p,S} h_S}[T_S(x) - T_C(x)] - \frac{k_A}{\rho_S c_{p,S} h_S}[T_S(x) - T_A(x)] - \frac{2}{\rho_S c_{p,S} h_S}\left[\frac{\sigma[T_S(x)^4 - T_I(x)^4]}{(1/\varepsilon_S) + (1/\varepsilon_I) - 1}\right] + \frac{1}{\rho_S c_{p,S} h_S}[-\Delta H(x)R(x) + j(x)U] \quad (20)$$

$$\frac{\partial}{\partial x}[T_S(0)] = 0, \qquad \frac{\partial}{\partial x}[T_S(L)] = 0 \quad (21)$$

$$\frac{\partial}{\partial t}[T_I(x)] = \frac{\lambda_I}{\rho_I c_{p,I}}\frac{\partial^2}{\partial x^2}[T_I(x)] - \frac{k_C}{\rho_I c_{p,I} h_I}[T_I(x) - T_C(x)] - \frac{k_A}{\rho_I c_{p,I} h_I}[T_I(x) - T_A(x)] + \frac{2}{\rho_I c_{p,I} h_I}\left[\frac{\sigma[T_S(x)^4 - T_I(x)^4]}{(1/\varepsilon_S) + (1/\varepsilon_I) - 1}\right] \quad (22)$$

$$\frac{\partial}{\partial x}[T_I(0)] = 0, \qquad \frac{\partial}{\partial x}[T_I(L)] = 0 \quad (23)$$

$$k_C = Nu_C\frac{\lambda_C}{d_{h,C}}, \qquad k_A = Nu_A\frac{\lambda_A}{d_{h,A}} \quad (24)$$

$$d_{h,C} = \frac{2Wh_C}{W + h_C}, \qquad d_{h,A} = \frac{2Wh_A}{W + h_A} \quad (25)$$

3. Simulation results and discussion

The system of partial differential and algebraic Eqs. (1)–(4) and (7)–(25) presented in the previous sections is solved via the finite difference method using gPROMS Model Builder 2.3.5 [13]. The model input parameters and the operating conditions applied for the steady state simulations are introduced in Section 3.1. Section 3.2 discusses the effects of current density and temperature on the cell potential while Section 3.3 presents the spatially distributed simulation results.

3.1. Input parameters and inlet operating conditions

In addition to the input parameters such as cell geometry, material properties and inlet stream conditions, the IT-SOEC model described in the previous sections involves two degrees of freedom. Here, average current density and steam utilisation factor are adopted as the user-defined parameters from which the inlet molar flux of steam is determined. The average current density is directly proportional to the H_2 production rate while the steam utilisation factor is the fraction of total inlet steam consumed by the reaction. Although a low steam utilisation factor is preferred from the stack efficiency point of view, a reduction in the steam utilisation factor results in an increased cathode stream flow rate for a given H_2 production rate. In the system design, the selection of the steam utilisation factor must take into account the efficiency of the entire system as well as the added investment cost involved in accommodating the increased cathode stream flow rate. It is also important for the steam utilisation factor to be low enough to avoid a significant increase in the cathode concentration overpotential caused by steam starvation near the cell outlet. Here, a value of 80% is chosen. Table 3 presents the model input parameters selected for the steady state simulations including the cell geometry, the material properties, the cathode stream inlet temperature and composition, the operating pressure, the average current density and the steam utilisation factor. Due to the oxidising environment that pure steam would create at elevated temperatures, such a gas composition is not recommended for the cathode stream in an SOEC. Instead, conceptual system designs may consider the recirculation of some of the product hydrogen, which is mixed with the steam at the inlet to ensure reducing conditions [10,14,21]. Here, 10 mol% H_2 in the cathode inlet stream is assumed suf-

Table 3
Model input parameters and operating conditions

Cathode channel height, h_C	0.001 m
Anode channel height, h_A	0.001 m
Solid structure thickness, h_S	570×10^{-6} m
Interconnect thickness, h_I	500×10^{-6} m
Cell length, L	0.4 m
Cell width, W	0.1 m
Cathode thickness, $\tau_{cathode}$	500×10^{-6} m
Electrolyte thickness, $\tau_{electrolyte}$	20×10^{-6} m
Anode thickness, τ_{anode}	50×10^{-6} m
Cathode electric conductivity, $\sigma_{cathode}$	$80 \times 10^3\ \Omega^{-1}\ m^{-1}$
Electrolyte ionic conductivity, $\sigma_{electrolyte}$	$33.4 \times 10^3 \exp(-10.3\times10^3/T_S)\ \Omega^{-1}\ m^{-1}$
Anode electric conductivity, σ_{anode}	$8.4 \times 10^3\ \Omega^{-1}\ m^{-1}$
Cathode average effective diffusivity, $D_{eff,cathode}$	$36.6 \times 10^{-6}\ m^{-2}\ s^{-1}$
Solid structure emissivity, ε_S	0.8
Interconnect emissivity, ε_I	0.1
Solid structure heat capacity, $C_{p,S}$	$500\ J\ kg^{-1}\ K^{-1}$
Interconnect heat capacity, $C_{p,I}$	$500\ J\ kg^{-1}\ K^{-1}$
Solid structure thermal conductivity, λ_S	$2\ J\ m^{-1}\ s^{-1}\ K^{-1}$
Interconnect thermal conductivity, λ_I	$25\ J\ m^{-1}\ s^{-1}\ K^{-1}$
Solid structure density, ρ_S	$5900\ kg\ m^{-3}$
Interconnect density, ρ_I	$8000\ kg\ m^{-3}$
Cathode stream Nusselt number, Nu_C	3.09
Anode stream Nusselt number, Nu_A	3.09
Transfer coefficient, α	0.5
Cathode stream inlet temperature, T_C^0	1023 K
Cathode stream inlet composition	10 mol% H_2/90 mol% H_2O
Anode stream composition	100 mol% O_2
Operating pressure	0.1×10^6 Pa
Average current density	$5000\ A\ m^{-2}$
Steam utilisation factor	80%

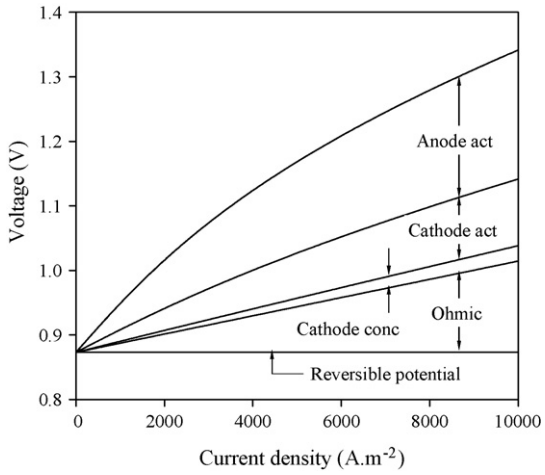

Fig. 3. Reversible potential and irreversible losses as a function of current density at 1023 K. The gas compositions are equivalent to those at the cell inlet.

ficient [10]. Note that the model assumes the cell with a total length of 0.4 m, comprising of four individual parts connected in series, each with a dimension of 0.1 m × 0.1 m. The cell geometry and material properties are based on the values employed in a previously developed IT-SOFC model [7].

3.2. Effects of operating conditions on the cell potential

The selection of operating conditions for an SOEC can significantly influence the irreversible losses, altering the cell potential required for the electrolysis. Such effect is illustrated in Figs. 3 and 4, respectively, showing the cell potential as a function of current density and temperature. Note that these curves do not result from the full IT-SOEC model described in Section 2. Instead, Figs. 3 and 4 are produced using only the electrochemical model in Section 2.1, taking the cathode and anode stream compositions to be equivalent to those at the cell inlet.

Fig. 3 shows the predicted cell potential at 1023 K, indicating the contributions of the reversible potential and each form of irreversible losses. As can be seen, all the irreversible losses increase with current density. At 8000 A m^{-2}, the cell potential is around 1.28 V with the anode activation overpotential being the largest form of irreversible losses at around 0.18 V, followed by the Ohmic losses and the cathode activation overpotential at around 0.11 V and 0.09 V, respectively. In spite of the cathode-supported nature of the cell, the cathode concentration overpotential contributes less than 0.02 V to the cell potential at 8000 A m^{-2}. While the Ohmic losses show essentially linear increase with the current density, the activation overpotentials follow non-linear paths. Although a decreased current density allows the reduction in the cell potential and consequent decrease in electrical energy consumption, a low current density also results in a low H_2 production rate per unit cell area. Therefore, the selection of the current density at which the cell should be operated must consider the operating cost involved with the electrical energy consumption of the stack as well as the investment cost associated with the stack area required in supporting the specified H_2 production rate.

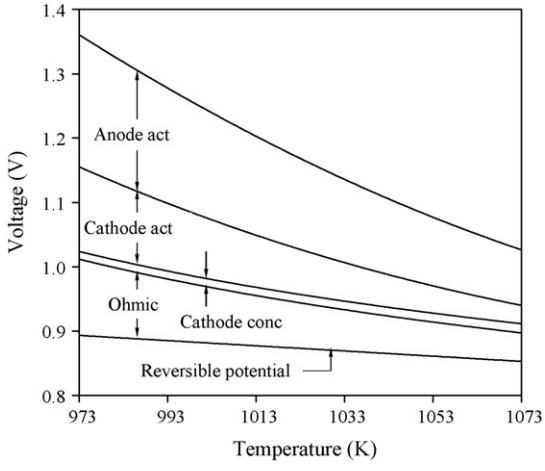

Fig. 4. Reversible potential and irreversible losses as a function of temperature at 5000 A m^{-2}. The gas compositions are equivalent to those at the cell inlet.

Another operating condition to be selected in the design of an SOEC is the operating temperature. The reversible potential and irreversible losses are illustrated as a function of temperature in Fig. 4. Except for the cathode concentration overpotential, which remains approximately constant, all the irreversible losses decrease with temperature. Between 973 and 1073 K, the cell potential is significantly decreased from around 1.36 to 1.03 V, with the combined irreversible losses being reduced by more than 60%. As expected from thermodynamics, the reversible potential given by the Nernst equation also decreases with temperature. The selection of the operating temperature must again consider the operating cost linked with the electrical energy consumption of the stack. In addition, it must account for the investment cost involved in creating both a stack with the required thermal stability as well as the whole system that needs to operate at that specified temperature. If the use of waste heat from external sources is considered, the temperature of such a heat stream would also become an important factor.

3.3. IT-SOEC operation

This section presents the spatially distributed steady state simulation results obtained by solving the full IT-SOEC model described in Section 2. Profiles of the temperature, the reversible potential, the irreversible losses and the local current density are illustrated along the cell. Different modes of operation for an SOEC are explained and the issues associated with the thermal management of the cells are discussed.

Fig. 5 shows the temperature distribution along the cathode stream for the cell operation at average current densities of 5000 A m^{-2} and 7000 A m^{-2}, maintaining all other conditions consistent with Table 3. Note that the cathode stream temperature changes rapidly after the cell entry, reaching the temperature of other cell components within a very short distance of the inlet. As can be seen in Fig. 5, the temperature gradient depends significantly on the average current density. While the temperature decreases along the cell at 5000 A m^{-2}, the heat accumulation causes the cell temperature to increase towards the outlet in the 7000 A m^{-2} case. This dependence of the cell temperature gra-

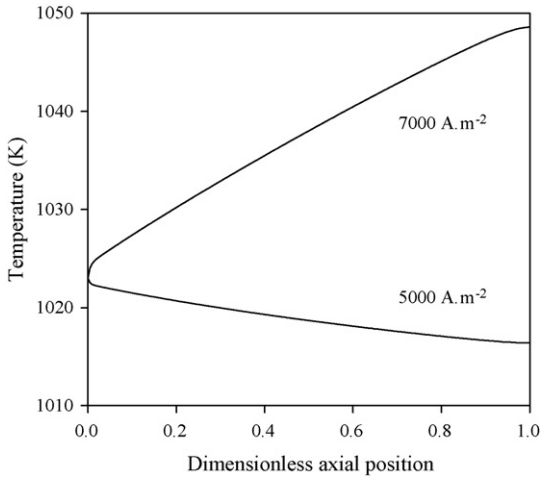

Fig. 5. Cathode stream temperature along the cell for average current densities of 5000 A m^{-2} and 7000 A m^{-2} and the conditions in Table 3.

dient on the average current density, or the hydrogen production rate, thus calls for a strict cell temperature control.

The effect of current density on the temperature gradient can be explained by considering the thermal energy (per mole of H_2) consumed by the endothermic electrolysis reaction ($T\Delta S$) and that produced by the irreversible losses within the cell ($2F\eta_{total}$), which are illustrated in Fig. 6 as a function of current density at 1023 K. Note that these results are produced using only the electrochemical model in Section 2.1. The cathode stream composition, averaged over the cell length, is taken as 46 mol% H_2/54 mol% H_2O, and employed here together with the anode stream composition of 100 mol% O_2. As can be seen, at 5000 A m^{-2} the irreversible losses are not sufficient to provide the entire thermal energy consumed by the reaction. Consequently, the temperature is decreased as the reaction proceeds along the cell. At 7000 A m^{-2}, however, the excess heat produced via the irreversible losses causes the temperature to rise towards the cell outlet. The curves intersect at around

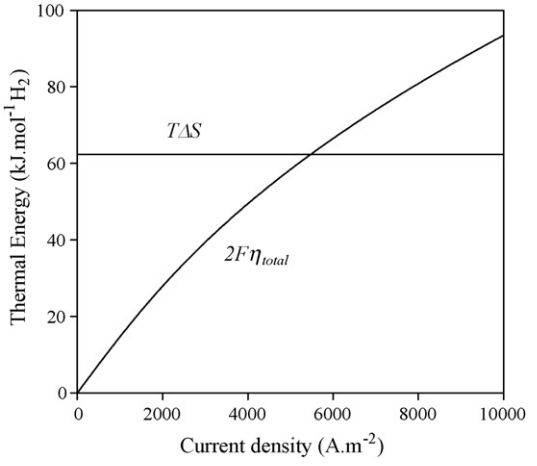

Fig. 6. Thermal energy (per mole of H_2) consumed by the reaction ($T\Delta S$) and that produced by the irreversible losses ($2F\eta_{total}$) as a function of current density at 1023 K. The stream compositions are taken as 46 mol% H_2 / 54 mol% H_2O and 100 mol% O_2.

5500 A m^{-2}, where the thermal energy consumed by the reaction is equivalent to that produced by the irreversible losses. Such condition corresponds to a thermoneutral operation in which the entire enthalpy change in the electrolysis is matched by the electrical energy input to the cell.

In the view of energy efficiency and operating cost, an SOEC stack should preferably be driven at current densities below that of the thermoneutral operation. Such a condition, which results in an endothermic stack operation, allows the opportunity to recover waste heat from external processes to partly replace the electrical energy consumption of the stack. However, as mentioned previously, the operation of the stack at lower current densities requires a larger stack area to support a given H_2 production rate, involving higher investment cost. The use of heat from external sources also involves extra capital cost in the form of additional equipment. One point to note at this stage is that the curves on Fig. 6 correspond only to the cell operation under specified temperature and stream compositions. In an actual SOEC, these variables as well as the local current densities change along the cell. Therefore, imposing an endothermic condition, for example, at the inlet would not necessarily ensure the entire cell to operate under the same mode.

As previously mentioned, the dependence of the cell temperature distribution on the average current density poses some challenges in terms of stack temperature control. Although the operating point of an SOEC stack is not expected to change dramatically if using grid or nuclear electrical powers as the input, such is not the case if the input power varies significantly with time. It is thus essential to have an appropriate temperature control strategy in place. The implementation of an effective control strategy should avoid significant thermal excursions in the stack, preventing the fracture of its components and ensuring that the operating mode of the stack remains constant. Avoiding transitions in the operating mode is important as the system requirements vary depending on whether the stack is employed in an endothermic, thermoneutral or exothermic operation in which the average current density is above the thermoneutral point. One possible solution in achieving the control requirements would be to modify the SOEC design such that one more degree of freedom is available to control the stack temperature. As can be seen in [16], in the case of SOFCs, the stack temperature is often controlled by varying the air flow through the cell. Such strategy may potentially be applied in the case of an SOEC where the introduction of air flow through the cell could both force the O_2 product out of the anode channel and aid in controlling the temperature. Such air flow would, however, cause the stack temperature to decrease and its effect needs to be quantified. Different SOEC concepts with the aim of addressing the issue of temperature control are the focus of a future publication.

Figs. 7 and 8 show the contributions of the reversible potential and irreversible losses on the cell potential for the conditions in Table 3, at the average current densities of 5000 A m^{-2} and 7000 A m^{-2}, respectively. In both cases, the activation overpotentials dominate the irreversible losses while the concentration overpotentials remain insignificant along the cell. For the 7000 A m^{-2} case, the thermodynamics predict the reversible

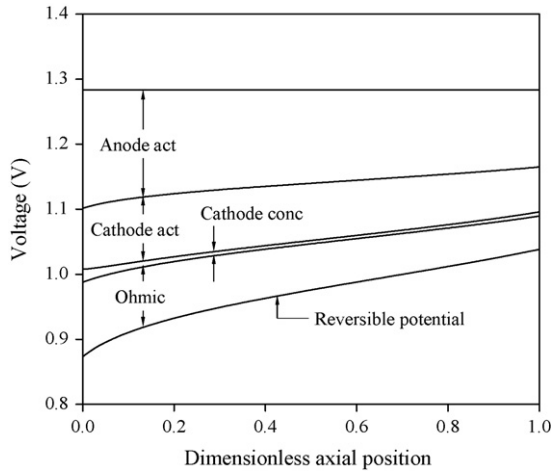

Fig. 7. Reversible potential and irreversible losses along the cell for the average current density of 5000 A m^{-2} and for the conditions in Table 3.

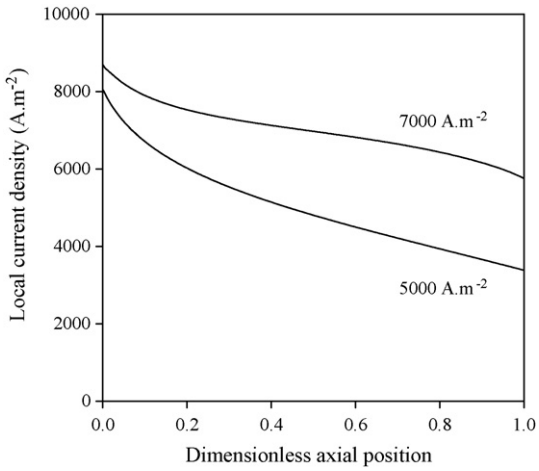

Fig. 9. Local current density along the cell for the average current densities of 5000 A m^{-2} and 7000 A m^{-2}, and for the conditions in Table 3.

potential to decrease as the cell temperature is raised along the cell. Fig. 8, however, indicates an increase in the reversible potential along the cell due to the change in the cathode stream composition. The similarity between the reversible potential distributions in Figs. 7 and 8, in spite of the difference in the temperature distributions for the two cases, suggests that the reversible potential is more strongly coupled with the stream composition than with the cell temperature in the range of the analysis. Figs. 7 and 8 also show the overall reduction in the irreversible losses along the cell. Although a negative temperature gradient is observed in Fig. 5 for the average current density of 5000 A m^{-2}, Ohmic losses and the activation overpotentials are decreased along the cell in Fig. 7. This is due to the rapid reduction in the local current density, indicating a significant decrease in the H_2 production rate along the cell. The local current density distributions are shown in Fig. 9 for the average current densities of 5000 A m^{-2} and 7000 A m^{-2}.

The steady state simulations of the full IT-SOEC model for the conditions in Table 3 predict cell potentials of 1.28 V and 1.30 V for the average current densities of 5000 A m^{-2} and 7000 A m^{-2}, respectively. For the 7000 A m^{-2} case in which the outlet gas temperature is above the inlet temperature, it may be possible to bring the inlet stream up to the required temperature entirely through heat recovery from the outlet streams. With such a system design, electricity is the only source of energy required for the stacks. The predicted 1.30 V equates to an electricity consumption of around 250.1 kJ mol^{-1} H_2 or 3.1 kW h per normal m^3 of H_2. This is significantly lower than 4.2 kW h per normal m^3 of H_2, which is the electricity consumption of one of the most efficient low temperature electrolysis stacks commercially available today [22]. Neither values include parasitic energy consumption within the system.

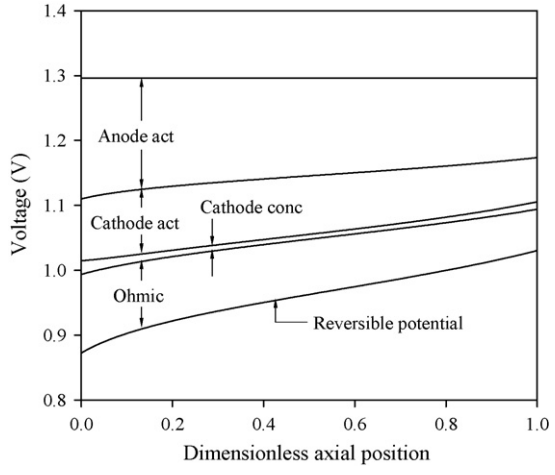

Fig. 8. Reversible potential and irreversible losses along the cell for the average current density of 7000 A m^{-2} and for the conditions in Table 3.

4. Conclusions

A one-dimensional distributed dynamic model of a cathode-supported planar IT-SOEC stack has been presented. The model has been employed to study both the steady state behaviour of an SOEC as well as its electrochemical performance at various current densities and temperatures. Electrochemical performance analysis alone has shown that, for the case where the cathode and anode inlet stream compositions are equivalent to 10 mol% H_2 / 90 mol% H_2O and 100 mol% O_2 respectively, both a decrease in current density and an increase in the cell temperature result in a reduction of the combined irreversible losses and thus a decrease in the electrical potential. Activation overpotentials were observed to provide the largest contributions to the irreversible losses while the concentration overpotentials remained insignificant throughout, in spite of the electrode-supported nature of the cell. The steady state performance analysis of the cell has shown that for an average current density of 7000 A m^{-2} and a cathode inlet stream temperature of 1023 K, the cell potential is 1.30 V, which corresponds to an electricity consumption of around 3.1 kW h per normal m^3 of H_2. This is significantly smaller than those of low temperature stacks commercially available today. However, the dependence of the cell temperature distribution on the average current density calls for a strict temperature control, especially during dynamic opera-

tion. Alternative concepts to accommodate such a feature and their dynamic behaviour will be presented in the future.

References

[1] D.L. Stojic, M.P. Marceta, S.P. Sovilj, S.S. Miljanic, J. Power Sources 118 (2003) 315–319.
[2] S.R. Turns, An Introduction to Combustion: Concepts and Applications, second ed., McGraw-Hill, 2000.
[3] W. Donitz, E. Erdle, R. Streicher, in: H. Wendt (Ed.), Electrochemical Hydrogen Technologies, Elsevier Science Publishers, 1990, pp. 213–258.
[4] T. Kobayashi, K. Abe, Y. Ukyo, H. Matsumoto, Solid State Ionics 138 (2001) 243–251.
[5] T. Schober, Solid State Ionics 139 (2001) 95–104.
[6] H. Matsumoto, M. Okubo, S. Hamajima, K. Katahira, H. Iwahara, Solid State Ionics 152–153 (2002) 715–720.
[7] P. Aguiar, C.S. Adjiman, N.P. Brandon, J. Power Sources 138 (2004) 120–136.
[8] W. Donitz, E. Erdle, Int. J. Hydrogen Energy 10 (1985) 291–295.
[9] R. Hino, K. Haga, H. Aita, K. Sekita, Nucl. Eng. Des. 233 (2004) 363–375.
[10] J.S. Herring, P. Lessing, J.E. O'Brien, C. Stoots, J. Hartvigsen, S. Elangovan, Proceedings of the 2nd Information Exchange Meeting on Nuclear Production of Hydrogen, 2003, pp. 183–200.
[11] W. Doenitz, R. Schmidberger, Int. J. Hydrogen Energy 7 (1982) 321–330.
[12] J. Larminie, A. Dicks, Fuel Cell Systems Explained, second ed., Wiley, 2003.
[13] Process Systems Enterprise Ltd., gPROMS Introductory User Guide, 2002.
[14] F.J. Salzano, G. Skaperdas, A. Mezzina, Int. J. Hydrogen Energy 10 (1985) 801–809.
[15] W. Doenitz, R. Schmidberger, E. Steinheil, R. Streicher, Int. J. Hydrogen Energy 5 (1980) 55–63.
[16] P. Aguiar, C.S. Adjiman, N.P. Brandon, J. Power Sources 147 (2005) 136–147.
[17] P. Iora, P. Aguiar, C.S. Adjiman, N.P. Brandon, Chem. Eng. Sci. 60 (2005) 2963–2975.
[18] U.G. Bossel, Facts and Figures, Final Report on SOFC Data, IEA Report, Swiss Federal Office of Energy, Operating Agent Task II (1992).
[19] S.H. Chan, K.A. Khor, Z.T. Xia, J. Power Sources 93 (2001) 130–140.
[20] J. Kim, A.V. Virkar, K. Fung, K. Mehta, S.C. Singhal, J. Electrochemical Soc. 146 (1999) 69–78.
[21] G. Rodriguez, T. Pinteaux, Proceedings of the 1st European Hydrogen Energy Conference, 2003, CD-ROM.
[22] Hydrogenics Corporation, http://www.hydrogenics.com, Accessed on 04/09/2006.